

Potential PeVatron supernova remnant G106.3+2.7 seen in the highest-energy gamma rays

The Tibet AS γ Collaboration

M. Amenomori¹, Y. W. Bao², X. J. Bi³, D. Chen^{4*}, T. L. Chen⁵, W. Y. Chen³, Xu Chen³, Y. Chen², Cirennima⁵, S. W. Cui⁶, Danzengluobu⁵, L. K. Ding³, J. H. Fang^{3,7}, K. Fang³, C. F. Feng⁸, Zhaoyang Feng³, Z. Y. Feng⁹, Qi Gao⁵, Q. B. Gou³, Y. Q. Guo³, Y. Y. Guo³, H. H. He³, Z. T. He⁶, K. Hibino¹⁰, N. Hotta¹¹, Haibing Hu⁵, H. B. Hu³, J. Huang³, H. Y. Jia⁹, L. Jiang³, H. B. Jin⁴, K. Kasahara¹², Y. Katayose¹³, C. Kato¹⁴, S. Kato¹⁵, K. Kawata¹⁵, W. Kihara¹⁴, Y. Ko¹⁴, M. Kozai¹⁶, Labaciren⁵, G. M. Le¹⁷, A. F. Li^{18,8,3}, H. J. Li⁵, W. J. Li^{3,9}, Y. H. Lin^{3,7}, B. Liu¹⁹, C. Liu³, J. S. Liu³, M. Y. Liu⁵, W. Liu³, Y.-Q. Lou^{20,21,22}, H. Lu³, X. R. Meng⁵, K. Munakata¹⁴, H. Nakada¹³, Y. Nakamura³, H. Nanjo¹, M. Nishizawa²³, M. Ohnishi¹⁵, T. Ohura¹³, S. Ozawa²⁴, X. L. Qian²⁵, X. B. Qu²⁶, T. Saito²⁷, M. Sakata²⁸, T. K. Sako^{15*}, J. Shao^{3,8}, M. Shibata¹³, A. Shiomi²⁹, H. Sugimoto³⁰, W. Takano¹⁰, M. Takita¹⁵, Y. H. Tan³, N. Tateyama¹⁰, S. Torii³¹, H. Tsuchiya³², S. Udo¹⁰, H. Wang³, H. R. Wu³, L. Xue⁸, Y. Yamamoto^{28†}, Z. Yang³, Y. Yokoe¹⁵, A. F. Yuan⁵, L. M. Zhai⁴, H. M. Zhang³, J. L. Zhang³, X. Zhang², X. Y. Zhang⁸, Y. Zhang³, Yi Zhang³³, Ying Zhang³, S. P. Zhao³, Zhaxisangzhu⁵ and X. X. Zhou⁹

¹Department of Physics, Hirosaki University, Hirosaki 036-8561, Japan

²School of Astronomy and Space Science, Nanjing University, Nanjing 210093, China

³Key Laboratory of Particle Astrophysics, Institute of High Energy Physics, Chinese Academy of Sciences, Beijing 100049, China

⁴National Astronomical Observatories, Chinese Academy of Sciences, Beijing 100012, China

⁵Physics Department of Science School, Tibet University, Lhasa 850000, China

⁶Department of Physics, Hebei Normal University, Shijiazhuang 050016, China

⁷University of Chinese Academy of Sciences, Beijing 100049, China

⁸Institute of Frontier and Interdisciplinary Science and Key Laboratory of Particle Physics and Particle Irradiation (MOE), Shandong University, Qingdao 266237, China

⁹Institute of Modern Physics, SouthWest Jiaotong University, Chengdu 610031, China

¹⁰Faculty of Engineering, Kanagawa University, Yokohama 221-8686, Japan

¹¹Faculty of Education, Utsunomiya University, Utsunomiya 321-8505, Japan

¹²Faculty of Systems Engineering, Shibaura Institute of Technology, Omiya 330-8570, Japan

¹³Faculty of Engineering, Yokohama National University, Yokohama 240-8501, Japan

¹⁴Department of Physics, Shinshu University, Matsumoto 390-8621, Japan

¹⁵Institute for Cosmic Ray Research, University of Tokyo, Kashiwa 277-8582, Japan

¹⁶Institute of Space and Astronautical Science, Japan Aerospace Exploration Agency (ISAS/JAXA), Sagami-hara 252-5210, Japan

¹⁷National Center for Space Weather, China Meteorological Administration, Beijing 100081, China

¹⁸School of Information Science and Engineering, Shandong Agriculture University, Taian 271018, China

[†]deceased

- ¹⁹Department of Astronomy, School of Physical Sciences, University of Science and Technology of China, Hefei, Anhui 230026, China
- ²⁰Department of Physics and Tsinghua Centre for Astrophysics (THCA), Tsinghua University, Beijing 100084, China
- ²¹Tsinghua University-National Astronomical Observatories of China (NAOC) Joint Research Center for Astrophysics, Tsinghua University, Beijing 100084, China
- ²²Department of Astronomy, Tsinghua University, Beijing 100084, China
- ²³National Institute of Informatics, Tokyo 101-8430, Japan
- ²⁴National Institute of Information and Communications Technology, Tokyo 184-8795, Japan
- ²⁵Department of Mechanical and Electrical Engineering, Shangdong Management University, Jinan 250357, China
- ²⁶College of Science, China University of Petroleum, Qingdao 266555, China
- ²⁷Tokyo Metropolitan College of Industrial Technology, Tokyo 116-8523, Japan
- ²⁸Department of Physics, Konan University, Kobe 658-8501, Japan
- ²⁹College of Industrial Technology, Nihon University, Narashino 275-8575, Japan
- ³⁰Shonan Institute of Technology, Fujisawa 251-8511, Japan
- ³¹Research Institute for Science and Engineering, Waseda University, Tokyo 169-8555, Japan
- ³²Japan Atomic Energy Agency, Tokai-mura 319-1195, Japan
- ³³Key Laboratory of Dark Matter and Space Astronomy, Purple Mountain Observatory, Chinese Academy of Sciences, Nanjing 210034, China

Cosmic rays (protons and other atomic nuclei) are believed to gain energies of petaelectronvolts (PeV) and beyond at astrophysical particle accelerators called ‘PeVatrons’ inside our Galaxy. Although a characteristic feature of a PeVatron is expected to be a hard gamma-ray energy spectrum that extends beyond 100 teraelectronvolts (TeV) without a cutoff, none of the currently known sources exhibits such a spectrum due to the low maximum energy of accelerated cosmic rays or insufficient detector sensitivity around 100 TeV. Here we report the observation of gamma-ray emission from the supernova remnant G106.3+2.7 [refs. ^{1,5}] above 10 TeV. This work provides flux data points up to and above 100 TeV and indicates that the very-high-energy gamma-ray emission above 10 TeV is well correlated with a molecular cloud³ rather than the pulsar PSR J2229+6114 [refs. ^{4,5,7–9}]. Regarding the gamma-ray emission mechanism of G106.3+2.7, this morphological feature appears to favor a hadronic origin via the π^0 decay caused by accelerated relativistic protons⁹ over a leptonic one via the inverse-Compton scattering by relativistic electrons^{10,11}. Furthermore, we point out that an X-ray flux upper limit on the synchrotron spectrum would provide important information to firmly establish the hadronic scenario as the mechanism of particle acceleration at the source.

The Milagro experiment reported an elongated gamma-ray source MGRO J2228+61 coincident with PSR J2229+6114 [refs. ^{12,13}] at 35 TeV. Meanwhile, the VERITAS experiment detected gamma-ray emissions above 1 TeV from the supernova remnant (SNR) G106.3+2.7 with a flux of $\sim 5\%$ Crab and named the source VER J2227+608 [ref. ⁴]. Recently the HAWC experiment observed G106.3+2.7 and reported a best-fit spectrum with an error band above 40 TeV [ref. ¹⁵]. The centroid of VER J2227+608, 0.4° away from PSR J2229+6114 in the southwest direction, is consistent with that of MGRO J2228+61 and the HAWC centroid within statistical and systematic uncertainties. In this work, we use data obtained by the Tibet air shower array combined with the muon detector array (Tibet AS+MD) during 719 live days from 2014 February to 2017 May to observe high-energy gamma-ray emissions from the region around G106.3+2.7. Figure 1 shows the detection significance map around G106.3+2.7 above 10 TeV, smoothed by the search window size (see Methods). The events can be well fitted with a symmetrical 2D Gaussian function, and the centroid of gamma-ray emissions (a red filled star with a red position error circle) is at (R.A., Dec) = $(336.82^\circ \pm 0.16_{stat}^\circ, 60.85^\circ \pm 0.10_{stat}^\circ)$, coincident with the location of a molecular cloud revealed by ^{12}CO ($J = 1 - 0$) emissions (green contours)³ overlying the black radio contours^{16,17} of the SNR, and is away from PSR J2229+6114 by 0.44° in the southwest direction. The location of our centroid is also consistent with those of VERITAS⁴ and HAWC¹⁵. Given the distance of 800 pc from the Earth to both PSR J2229+6114 and SNR G106.3+2.7, the distance from the pulsar to the gamma-ray emission centroid obtained by this work is estimated to be 6 pc. We estimate that our emission centroid deviates from the pulsar location at a confidence level of 3.1σ , based on the error of 0.14° including both statistical and systematic errors (see Methods). Note that the location of the HAWC centroid is consistent with both those of the Boomerang pulsar and the molecular cloud centroid, and that the centroids of VERITAS and Fermi are coincident with the location of molecular cloud as well as our centroid.

Figure 2 shows the distribution of the number of observed incident gamma-ray photons

above 10 TeV as a function of the opening angle between the estimated arrival direction and the gamma-ray emission centroid. Fitting the data with a Gaussian function, we estimate the 1σ extent of the source to be $\sigma_{\text{EXT}} = 0.24^\circ \pm 0.10_{\text{stat}}^\circ$, consistent with that estimated by VERITAS of 0.27° (0.18°) along the major (minor) axis.

Figure 3 shows the differential energy spectrum of gamma-ray emissions from G106.3+2.7 measured by this work (red filled squares and two red downward arrows for two upper limits). The values of our data points can be found in Supplementary Table 1. The detection significance above 10 TeV is calculated to be 6.1σ . This gamma-ray energy spectrum can be fitted by a single power law from 6 to 115 TeV as $dN/dE = N_0(E/40 \text{ TeV})^{-\Gamma}$ with $N_0 = (9.5 \pm 1.6_{\text{stat}}) \times 10^{-16} [\text{cm}^{-2} \text{ s}^{-1} \text{ TeV}^{-1}]$ and $\Gamma = 2.95 \pm 0.17_{\text{stat}}$ ($\chi^2/\text{ndf} = 2.5/5$), and extends above 100 TeV. The systematic error of N_0 is estimated to be $+40\%/-31\%$, resulting from the 12% uncertainty in the absolute energy scale. The flux data points of VERITAS (blue filled circles) are raised by a factor of 1.62 to account for the spill-over of gamma-ray signals outside their window size (see Methods). Our three flux data points below 20 TeV overlapping the energy range covered by the VERITAS flux points are statistically consistent with 1.62 times VERITAS's original best-fit power-law function reported in their paper⁴ at the 1.5σ level. Our spectrum is consistent with the HAWC spectrum; the χ^2/ndf between the HAWC best-fit power-law spectrum and our flux data points overlapping the energy range covered by HAWC is $3.0/2$, which corresponds to the 0.8σ level, when only our statistical errors are considered. In addition, our spectral index above 40 TeV is $\Gamma = 3.17 \pm 0.63_{\text{stat}}$, which is consistent with the HAWC index $\Gamma = 2.25 \pm 0.23_{\text{stat}}$ at the 1.4σ level.

As to the physical mechanism of the gamma-ray emission, both leptonic and hadronic models are possible at the moment; the HAWC observation allows for the possibility of a purely leptonic model, although Bayesian Information Criterion values obtained in fitting their gamma-ray spectrum together with the VERITAS spectrum suggested that a hadronic model is slightly preferred. We fit the multi-wavelength gamma-ray energy spectrum using the *naima* package², which allows us to estimate the parent particle spectrum so as to best reproduce the observed gamma-ray energy spectrum. For the energy distribution of the parent particles, we assume an exponential cut-off power-law form of $dN/dE \propto E^{-\alpha} \exp(-E/E_{\text{cut}})$. The best-fit gamma-ray spectra for hadronic and leptonic models are shown in Extended Data Figure 1, and the best-fit parameters are listed in Supplementary Table 2. In the hadronic model, we get $E_{\text{cut}} \sim 0.5 \text{ PeV}$ and $\alpha \sim 1.8$. The value of α falls between that predicted in the standard diffusive shock acceleration ($\alpha = 2$) and the asymptotic limit of the very efficient proton acceleration ($\alpha = 1.5$) [refs. ^{10,11}]. The total energy of protons with energies $>1 \text{ GeV}$ ($>0.5 \text{ PeV}$) is estimated to be $\sim 5.0 \times 10^{47} \text{ erg}$ ($3.0 \times 10^{46} \text{ erg}$) for a target gas density of 10 cm^{-3} . One might argue that, considering the estimated SNR age of 10 kyr, PeV protons escape the SNR much earlier than the present time in the standard theory of cosmic-ray acceleration. Given that $E_{\text{cut}} \sim 0.5 \text{ PeV}$ and that the maximum energy of protons remaining inside an SNR is proportional to $\tau^{-0.5}$ where τ is the SNR age²¹, protons should be accelerated up to $\sim 1.6 \text{ PeV}$ at $\tau = 1 \text{ kyr}$ in the case of G106.3+2.7. This suggests that the acceleration of protons at G106.3+2.7 should be efficient enough²¹ to push their maximum energy up to $\sim 1.6 \text{ PeV}$ during the SNR free expansion phase. In addition, G106.3+2.7 has a dense molecular cloud nearby indispensable for accelerated protons to produce TeV gamma rays

via π^0 production. With $\alpha \sim 1.8$, the proton energy spectrum does not appear softened, implying that protons may not be able to escape the SNR easily due to the suppression of the diffusion coefficient (see Supplementary Information). Future observations of the physical parameters of G106.3+2.7 such as the magnetic field and the particle density could provide useful information for these theoretical studies on its mechanisms of particle acceleration and confinement.

Alternatively, the observed gamma-ray emission might result from protons accelerated by the SNR up to 0.1 PeV and then reaccelerated up to 1 PeV by the adiabatic compression of the Boomerang PWN inside the SNR²². If the adiabatic compression ended at an age of 5 kyr as estimated in the paper, accelerated PeV protons need to travel a distance of 6 pc from the Boomerang PWN to the molecular cloud during the lapse time of $T = 5$ kyr until the present time. The diffusion coefficient of a 0.5 PeV proton in the interstellar medium with a magnetic field of 3 μG would be $D \sim 2 \times 10^{30} \text{ cm}^2/\text{s}$ [ref. ⁸], giving a diffusion length of $L \sim 2\sqrt{DT} = 380 \text{ pc}$ [ref. ²⁴] for $T = 5$ kyr. Since the diffusion length around an SNR could be shorter by a factor of 10 or more²⁵, we then estimate $L \lesssim 38 \text{ pc}$. Since this is much larger than 6 pc, it would be possible for 0.5 PeV protons to diffuse from the Boomerang PWN to the molecular cloud and emit TeV gamma rays through π^0 production. This scenario might not be natural, however, considering that TeV gamma-ray emissions have not been detected from other molecular cloud clumps around the source (see green contours in Figure 1) although protons should also be able to diffuse up to them, and that the proton spectrum needs to be kept hard with $\alpha \sim 1.8$ after the diffusion of 6 pc for $T = 5$ kyr.

In the leptonic model, we get $E_{\text{cut}} \sim 190 \text{ TeV}$, $\alpha \sim 2.3$ and the SNR magnetic field strength of $\sim 9 \mu\text{G}$. The total energy of relativistic electrons with energies $> 10 \text{ MeV}$ is estimated to be $\sim 1.4 \times 10^{47} \text{ erg}$. We estimate in the Supplementary Information that electrons need to be accelerated freshly within 1 kyr if they originate from the SNR, and that electrons provided by the Boomerang PWN are not likely to produce the observed gamma-ray emission in view of the energy budget and the gamma-ray morphology. The X-ray flux for the small 2'-radius region at PSR J2229+6114 has been measured in the 2–10 keV range⁹, while the X-ray flux for the extended region of our gamma-ray emission region with the 1σ extent of 0.24° has not been published yet, although X-ray data of the region observed by Suzaku, XMM-Newton and Chandra are publicly available²⁶. We point out that a flux upper limit on the synchrotron spectrum at the X-ray band would provide important information to rule out the leptonic scenario for particle acceleration at the gamma-ray source (see Supplementary Information Figure 1). In a scenario presented in previous papers^{27,28}, a supernova explosion occurred at or very close to the current location of radio pulsar PSR J2229+6114 rather than the center of SNR G106.3+2.7. Part of the initial shock wave that expanded to the north and east encountered a particularly dense H I cloud and was quickly decelerated, giving rise to a strong asymmetric reverse shock that moved back in the southwest direction. Around 6.6 kyr after the supernova explosion the reverse shock crushed and drove away the initial PWN that was forming around the pulsar, and afterwards a second nebula was formed, which is the current Boomerang PWN of age ~ 3.9 kyr. In this scenario, electrons that were contained in the initial PWN might be blown away by the reverse shock southwestward and somehow reaccelerated at the SNR shell up to very high energies, emitting gamma rays via inverse-Compton (IC) scattering. This

scenario, therefore, might become possible if the reverse shock velocity of $6 \text{ pc} / 3.9 \text{ kyr} \sim 1,500 \text{ km/s}$ is attainable at the source. It might also be possible for unknown nearby pulsars to contribute to the observed gamma-ray emission.

In addition, a hybrid (leptonic+hadronic) scenario might also be possible²⁹. If the birthplace of the pulsar was coincident with the location of the molecular cloud, both electrons and protons accelerated during the early age of the pulsar could contribute to the observed TeV gamma-ray emission via IC scattering and π^0 decay ($p + p \rightarrow \pi^0 \rightarrow 2\gamma$), respectively. This scenario might not be natural, however, since no enhancement of gamma-ray emission was observed by *Fermi* at the current location of the pulsar³ although VERITAS detected some gamma-ray excess events there⁴. If this scenario applies, the pulsar moved $\sim 0.4^\circ$ towards its current location with a transverse velocity of $\sim 570 \text{ km/s}$ during the age of 10 kyr. Future measurements of the pulsar velocity would be important to investigate the validity of this scenario.

It is known that the energy spectrum of hadronically-induced gamma rays rises steeply below $\sim 200 \text{ MeV}$ and approximately follows the energy spectrum of parent particles above a few GeV, resulting in a characteristic “ π^0 -decay bump” in the gamma-ray spectrum. Hopefully, further multi-wavelength observations in the future would establish the hadronic origin of gamma-ray emissions from SNR G106.3+2.7.

References

- [1] Joncas, G. & Higgs, L. A. The DRAO galactic-plane survey. II - Field at $l = 105^\circ$. *Astron. Astrophys. Suppl. Ser.* **82**, 113-144 (1990).
- [2] Pineault, S. & Joncas, G. G106.3+2.7: A supernova remnant in a late stage of evolution. *Astron. J.* **120**, 3218-3225 (2000).
- [3] Heyer, M. H. et al. The Five College Radio Astronomy Observatory CO survey of the outer galaxy. *Astrophys. J. Suppl. Ser.* **115**, 241-258 (1998).
- [4] Abdo, A. A. et al. *Fermi*/Large Area Telescope bright gamma-ray source list. *Astrophys. J. Suppl. Ser.* **183**, 46-66 (2009).
- [5] Abdo, A. A. et al. *Fermi* Large Area Telescope detection of pulsed γ -rays from the Vela-like pulsars PSR J1048–5832 and PSR J2229+6114. *Astrophys. J.* **706**, 1331-1340 (2009).
- [6] Halpern, J. P. et al. PSR J2229+6114: Discovery of an energetic young pulsar in the error box of the EGRET source 3EG J2227+6122. *Astrophys. J.* **552**, L125-L128 (2001).
- [7] Hartman, R. C. et al. The third EGRET catalog of high-energy gamma-ray sources. *Astrophys. J. Suppl. Ser.* **123**, 79-202 (1999).
- [8] Anderhub, H. et al. Search for very high energy gamma-ray emission from pulsar-pulsar wind nebula systems with the MAGIC Telescope. *Astrophys. J.* **710**, 828-835 (2010).
- [9] Naito, T. & Takahara, F. High energy gamma-ray emission from supernova remnants. *J. Phys. G: Nucl. Part. Phys.* **20**, 477-486 (1994).
- [10] Jones, F. C. Calculated spectrum of Inverse-Compton-scattered photons. *Phys. Rev.* **167**, 1159-1169 (1968).
- [11] Blumenthal, G. & Gould, R. Bremsstrahlung, synchrotron radiation, and Compton scattering of high-energy electrons traversing dilute gases. *Rev. of Mod. Phys.* **42**, 237-270 (1970).
- [12] Abdo, A. A. et al. TeV gamma-ray sources from a survey of the galactic plane with Milagro. *Astrophys. J.* **664**, L91-L94 (2007).
- [13] Abdo, A. A. et al. Milagro observations of multi-TeV emission from galactic sources in the *Fermi* Bright Source List. *Astrophys. J.* **700**, L127-L131 (2009).
- [14] Acciari, V. A. et al. Detection of extended VHE gamma ray emission from G106.3+2.7 with VERITAS. *Astrophys. J.* **703**, L6-L9 (2009).
- [15] Albert, A. et al. HAWC J2227+610 and its association with G106.3+2.7, a new potential galactic PeVatron. *Astrophys. J.* **896**, L29-L37 (2020).

- [16] Landecker, T. L. et al. The synthesis telescope at the Dominion Radio Astrophysical Observatory. *Astron. Astrophys. Suppl. Ser.* **145**, 509-524 (2000).
- [17] Taylor, A. R. et al. The Canadian galactic plane survey. *Astron. J.* **125**, 3145-3164 (2003).
- [18] Zabalza, V. naima: a Python package for inference of relativistic particle energy distributions from observed nonthermal spectra. Preprint at <https://arxiv.org/abs/1509.03319> (2015).
- [19] Malkov, M. A. Asymptotic particle spectra and plasma flows at strong shocks. *Astrophys. J.* **511**, L53-L56 (1999).
- [20] Berezhko, E. G. & Ellison, D. C. A simple model of nonlinear diffusive shock acceleration. *Astrophys. J.* **526**, 385-399 (1999).
- [21] Caprioli, D., Blasi, P. & Amato, E. On the escape of particles from cosmic ray modified shocks. *Mon. Not. R. Astron. Soc.* **396**, 2065-2073 (2009).
- [22] Ohira, Y., Kisaka, S. & Yamazaki, R. Pulsar wind nebulae inside supernova remnants as cosmic-ray PeVatrons. *Mon. Not. R. Astron. Soc.* **478**, 926-931 (2018).
- [23] Gabici, S., Aharonian, F. A. & Casanova, S. Broad-band non-thermal emission from molecular clouds illuminated by cosmic rays from nearby supernova remnants. *Mon. Not. R. Astron. Soc.* **396**, 1629-1639 (2009).
- [24] Atoyan, A. M., Aharonian, F. A. & Völk, H. J. Electrons and positrons in the galactic cosmic rays. *Phys. Rev. D.* **52**, 3265-3275 (1995).
- [25] Fujita, Y., Ohira, Y., Tanaka, S. J. & Takahara, F. Molecular clouds as a probe of cosmic-ray acceleration in a supernova remnant. *Astrophys. J.* **707**, L179-L183 (2009).
- [26] https://www.darts.isas.jaxa.jp/astro/suzaku/data/public_list/
- [27] Kothes, R., Reich, W. & Uyaniker, B. The Boomerang PWN G106.6+2.9 and the magnetic field structure in pulsar wind nebulae. *Astrophys. J.* **638**, 225-233 (2006).
- [28] Kothes, R., Uyaniker, B. & Pineault, S. The supernova remnant G106.3+2.7 and its pulsar-wind nebula: relics of triggered star formation in a complex environment. *Astrophys. J.* **560**, 236-243 (2001).
- [29] Bartko, H. & Bednarek, W. γ -ray emission from PWNe interacting with molecular clouds. *Mon. Not. R. Astron. Soc.* **385**, 1105-1109 (2008).
- [30] Xin, Y., Zeng, H., Liu, S., Fan, Y. & Wei, D. VER J2227+608: A hadronic PeVatron pulsar wind nebula? *Astrophys. J.* **885**, 162-167 (2019).

Correspondence

Correspondence and requests for materials should be addressed to T. K. S. (tsako@icrr.u-tokyo.ac.jp), D. C. (chending@nao.cas.cn), J. H. (huangjing@ihep.ac.cn), M. O. (ohnishi@icrr.u-tokyo.ac.jp), M. T. (takita@icrr.u-tokyo.ac.jp) and X. Z. (xiaozhang@nju.edu.cn).

Acknowledgments

The collaborative experiment of the Tibet Air Shower Arrays has been conducted under the auspices of the Ministry of Science and Technology of China and the Ministry of Foreign Affairs of Japan. This work was supported in part by a Grant-in-Aid for Scientific Research on Priority Areas from the Ministry of Education, Culture, Sports, Science and Technology, and by Grants-in-Aid for Science Research from the Japan Society for the Promotion of Science in Japan. This work is supported by the National Key R&D Program of China (No. 2016YFE0125500), the Grants from the National Natural Science Foundation of China (Nos. 11533007, 11673041, 11873065, 11773019, 11773014, 11633007, 11803011, and 11851305), and the Key Laboratory of Particle Astrophysics, Institute of High Energy Physics, CAS. The research presented in this paper has used data supplied through the Canadian Galactic Plane Survey. This work is also supported by the joint research program of the Institute for Cosmic Ray Research (ICRR), the University of Tokyo.

Author contributions

The whole Tibet AS γ collaboration contributed to the publication in terms of various aspects of the research ranging from hardware-related issues such as the design, construction, maintenance, calibration, etc. of the instrument to software-related issues such as data reduction, data analysis, MC simulation, astrophysical explanation, etc. D. C., J. H., M. O., T. K. S., M. T. and X. Z. analyzed the data and prepared the manuscript. All the authors discussed the results of this work and commented on the manuscript. Authors to whom correspondence should be addressed: T. K. S. (tsako@icrr.u-tokyo.ac.jp), D. C. (chending@nao.cas.cn), J. H. (huangjing@ihep.ac.cn), M. O. (ohnishi@icrr.u-tokyo.ac.jp), M. T. (takita@icrr.u-tokyo.ac.jp) and X. Z. (xiaozhang@nju.edu.cn).

Competing Interests

The authors declare no competing financial interests.

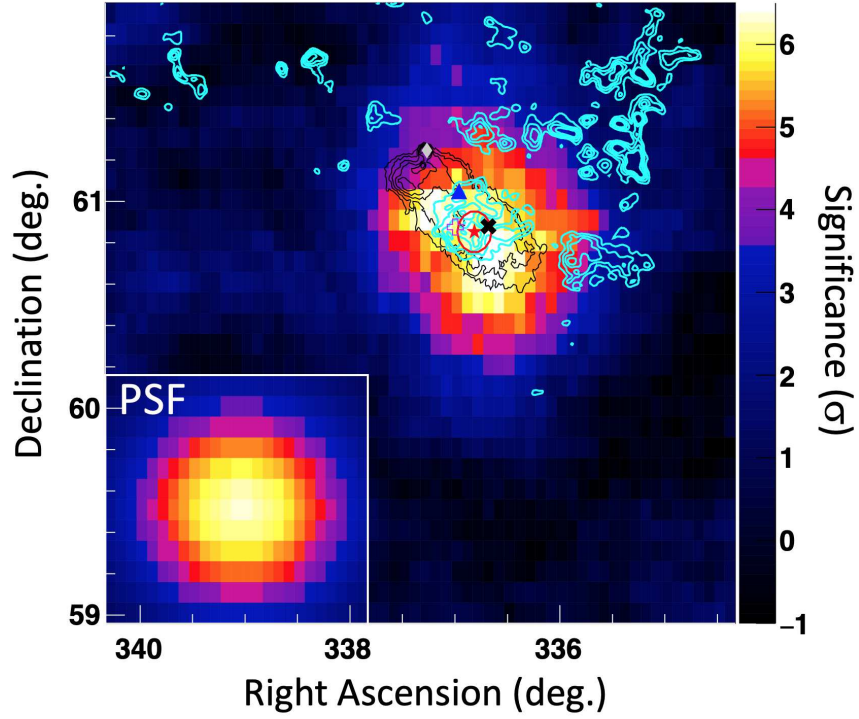


Figure 1: **Significance map around SNR G106.3+2.7 as observed by Tibet AS+MD above 10 TeV.** The inset figure shows our point spread function (PSF). The red filled star with a 1σ statistical position error circle is the centroid of gamma-ray emissions determined by this work, while the magenta open cross, the black X mark and the blue filled triangle are the centroids determined by VERITAS⁴, *Fermi*³ and HAWC¹⁵. The black contours indicate 1420 MHz radio emissions from the Dominion Radio Astrophysical Observatory Synthesis Telescope^{16,17}, and the cyan contours indicate ^{12}CO emissions from the Five College Radio Astronomy Observatory survey³. The gray filled diamond at the northeast corner of the radio emission marks the pulsar PSR J2229+6114.

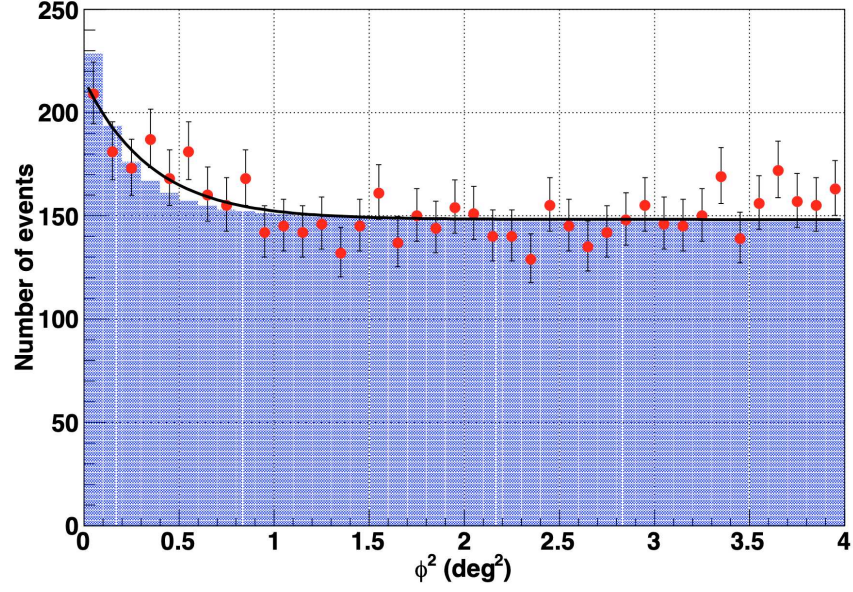


Figure 2: **Projected angular distribution of events observed above 10 TeV.** The horizontal axis ϕ^2 represents the square of the opening angle between the estimated event arrival direction and the centroid of gamma-ray emissions determined by this work. The red filled circles with 1σ statistical error bars are the experimental data with the best-fit black solid curve (see Methods). The blue histogram is the expected event distribution by our MC simulation assuming a point-like gamma-ray source.

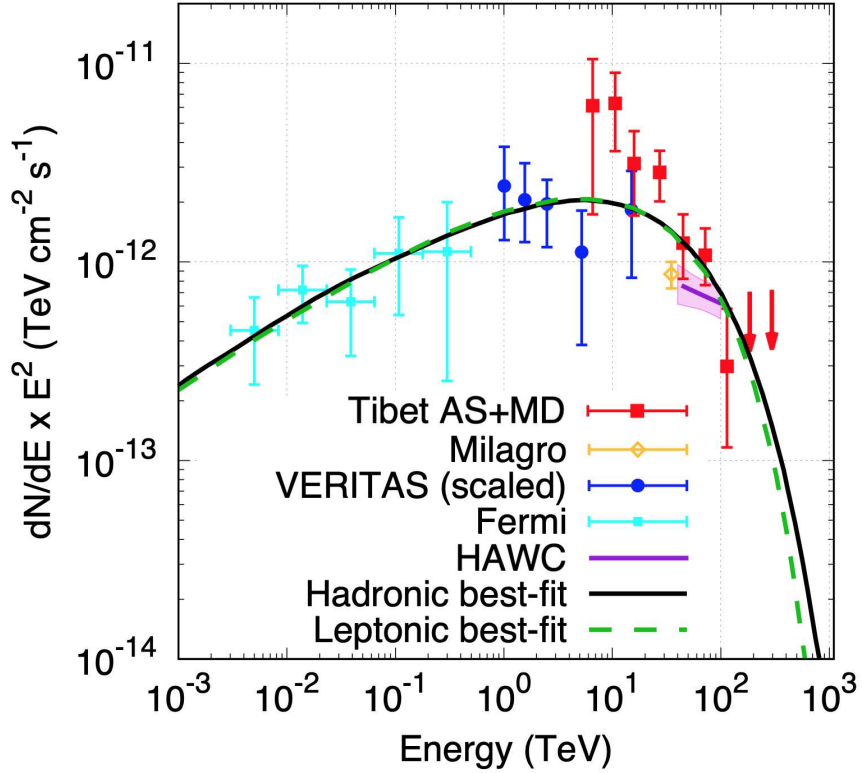


Figure 3: **Differential energy spectrum of gamma-ray emissions from SNR G106.3+2.7.** Red filled squares (Tibet AS+MD) represent data measured by this work with two 99% C.L. upper limits (downward red arrows), VERITAS⁴ (deep-blue filled circles), *Fermi*³ (sky-blue crosses), Milagro¹³ (an orange open diamond) and HAWC¹⁵ (a purple solid line with a shaded light purple area indicating the 1σ statistical error band). The error bars represent the 1σ statistical uncertainty. VERITAS's data points are raised by a factor of 1.62 from the original values (see Methods). The black solid (green dashed) line is the best-fit curve of the hadronic (leptonic) model for the combined data points of Tibet AS+MD, VERITAS and *Fermi*.

Methods

Experiment

The Tibet air-shower (AS) array has been in operation since 1990 at Yangbajing (90.522°E, 30.102°N; 4300 m above sea level) in Tibet, China, to observe cosmic rays and gamma rays above TeV energies³¹. Currently the AS array covers an area of $\sim 65,700 \text{ m}^2$ with 597 plastic scintillation counters placed on a 7.5-m square grid. An event trigger signal is issued on condition that any four-fold coincidence occur among the counters recording more than 0.6 particles each. The muon detector (MD) array has been in operation since 2014, covering an area of $3,450 \text{ m}^2$ with 64 water cells constructed approximately 2.4 m under the surface AS array. Air-shower muons with energies $\gtrsim 1 \text{ GeV}$ penetrate the soil overburden (~ 19 radiation lengths), while the soil shields electromagnetic components (e^\pm and γ) in air showers. Each water cell is filled with clear water with a depth of 1.5 m and its inner walls are covered with white Tyvek sheets. A 20-inch downward-facing photomultiplier tube put on the ceiling of each cell detects Cherenkov photons emitted by penetrating air-shower muons and reflected by the inner walls. Essentially, the MD array measures the number of muons in air showers that have triggered the AS array. The MD array records charge and timing information from the water cells in synchronization with event trigger signals issued by the AS array. Using the MD array, we can dramatically reduce background cosmic-ray events in gamma-ray observation by selecting muon-poor air-shower events, since air showers induced by background cosmic rays contain far more muons than those induced by primary gamma rays. Details are provided in our recent paper³² reporting the detection of cosmic gamma rays beyond 100 TeV.

MC simulation

Air showers are generated along the orbit of SNR G106.3+2.7 within a zenith-angle range of $\theta < 60^\circ$, assuming a gamma-ray energy spectrum with a power-law index of -2.9 above 0.3 TeV. CORSIKA v7.4000 [ref. ³³] is used for air-shower generation, with EPOS-LHC³⁴ for the high-energy hadronic interaction model and FLUKA v2011.2b [refs. ^{35,36}] for the low-energy hadronic interaction model. The generated air-shower particles are fed into the detector response simulation of the AS array and the MD array developed by GEANT v4.10.00 [ref. ³⁷]. Detailed simulation procedures can be found in our previous papers^{32,38}.

Data analysis

We estimate the arrival direction of a primary particle based on the relative timing information of the AS counters assuming a cone-shaped air-shower front. The slope of the cone is optimized by the MC simulation for gamma-ray observation. The angular resolution (50% containment) is estimated to be 0.5° and 0.2° for 10 TeV and 100 TeV gamma rays, respectively. The energy of a primary particle is reconstructed from the detected particle densities of the AS counters. Above 10 TeV, the lateral distribution of particle densities is fitted by the Nishimura-Kamata-Greisen (NKG) function, and then the particle density 50 m away from the air-shower axis (S_{50}) is calculated from the best-fit NKG function.

The reconstructed energy of the primary photon E_{rec} is thus obtained as a function of $S50$ and the zenith angle. The energy resolution is estimated to be 40% at 10 TeV and 20% at 100 TeV for primary gamma rays³⁹. The purity of E_{rec} bins for 10–16 TeV, 40–63 TeV and 100–158 TeV is 34%, 45% and 55%, respectively, while the contamination from lower (higher) energies is 39% (27%), 34% (21%) and 30% (15%), respectively. Below 10 TeV, the energy of a primary photon is reconstructed from $\Sigma\rho$, which is the sum of detected particle densities of all AS counters. The uncertainty in the absolute energy scale is estimated to be 12% [ref. ⁴⁰]. We evaluate our pointing precision at the declination of G106.3+2.7 by re-analyzing the source location of the Crab Nebula. After thinning out air-shower events so that the zenith-angle distribution of events is adjusted to that of G106.3+2.7, we fit the events in the same way described below. As a result, we obtain Crab’s position as (R.A., Dec.) = $(83.636^\circ \pm 0.137_{\text{stat}}^\circ, 21.991^\circ \pm 0.099_{\text{stat}}^\circ)$, and the deviation from the location of the Crab pulsar as $0.003^\circ \pm 0.137_{\text{stat}}^\circ$ in R.A. and $0.024^\circ \pm 0.099_{\text{stat}}^\circ$ in Dec. Therefore, we estimate the systematic pointing error for G106.3+2.7 as 0.10° in angular distance, although we expect that, as we accumulate statistics, the pointing error would be reduced to 0.023° (from our observation of the Crab Nebula³²), and further down to $< 0.011^\circ$ (from the analysis of the cosmic-ray shadow of the Moon⁴⁰).

The single peak of each MD cell is defined as the peak of the charge distribution of air-shower events that have triggered the AS array. The number of muons N_μ is calculated for each MD cell by dividing the recorded charge by the single peak, and then the total sum ΣN_μ is obtained for each air-shower event by summing up the N_μ values from all the MD cells.

The event selection criteria are the same as in our previous work³², except that we re-optimize the ΣN_μ condition, namely, $\Sigma N_\mu < 0.15 (\Sigma\rho)^{0.28}$ or $\Sigma N_\mu < 3.6 \times 10^{-4} (\Sigma\rho)^{1.4}$.

We adopt the Equi-Zenith-Angle method employed in our previous work^{40,41} to estimate background and gamma-ray excess counts. In this work, we take 20 off-sources with the same size and zenith angle as the on-source. The radius of the search window is optimized as $R_w = 6.9^\circ / \sqrt{\Sigma\rho}$, with a lower limit of 0.5° to keep >90% gamma-ray events at high energies $\gtrsim 100$ TeV where background contamination is low.

In Figure 1, the celestial region around SNR G106.3+2.7 is gridded in $0.1^\circ \times 0.1^\circ$ pixels. The significance value of each pixel is calculated¹ from background and gamma-ray excess counts within a search window centered at the pixel with the variable radius of R_w . To derive the centroid of gamma-ray emissions observed above 10 TeV, we fit the events within the $5^\circ \times 5^\circ$ region around the SNR using the unbinned maximum likelihood method.

To derive the 1σ extent of the source σ_{EXT} , we fit the data in Figure 2 with a Gaussian function:

$$G(\phi^2; A, \sigma_{\text{EXT}}) = A \exp \left[-\frac{\phi^2}{2(\sigma_{\text{PSF}}^2 + \sigma_{\text{EXT}}^2)} \right] + N_{\text{BG}}, \quad (1)$$

where A and σ_{EXT} are two fitting parameters, while the number of background events $N_{\text{BG}} = 148$ and the PSF of the instrument $\sigma_{\text{PSF}} = 0.35^\circ$ are estimated from the background cosmic-ray data and the gamma-ray MC simulation, respectively.

In Figure 3, VERITAS’s flux data points are raised by a factor of 1.62 from the original values⁴. Using the source extension reported by VERITAS with the 1σ angular extent of 0.27° (0.18°) along the major (minor) axis and their PSF of 0.11° , we estimate the spill-over

of gamma-ray signals outside their integration region of radius 0.32° to be 38.3%, which means that the total flux of the source should be higher by a factor of $1/(1 - 0.383) = 1.62$.

Data Availability

The data that support the plots within this paper and other findings of this study are available from the website of the Tibet AS γ Collaboration (<https://www.tibet-asg.org>) or from the corresponding authors upon reasonable request.

Code Availability

The codes used in this work are embedded within the analysis framework of the Tibet AS and MD array, and it is not practically possible to extract them. The codes, therefore, are not publicly available.

References

- [31] Amenomori, M. et al. Search for steady emission of 10-TeV gamma rays from the Crab Nebula, Cygnus X-3, and Hercules X-1 using the Tibet air shower array. *Phys. Rev. Lett.* **69**, 2468-2472 (1992).
- [32] Amenomori, M. et al. First detection of photons with energy beyond 100 TeV from an astrophysical source. *Phys. Rev. Lett.* **123**, 051101-1-051101-6 (2019).
- [33] Heck, D., Knapp, J., Capdevielle, J. N., Schatz, G. & Thouw, T. CORSIKA: A Monte Carlo code to simulate extensive air showers. *Report FZKA6019, Forschungszentrum Karlsruhe* (1998).
- [34] Pierog, T., Karpenko, Iu., Katzy, J. M., Yatsenko, E. & Werner, K. EPOS LHC: Test of collective hadronization with data measured at the CERN Large Hadron Collider. *Phys. Rev. C* **92**, 034906-1-034906-15 (2015).
- [35] Böhflen, T. T. et al. The FLUKA code: Developments and challenges for high energy and medical applications. *Nuclear Data Sheets*. **120**, 211-214 (2014)
- [36] Ferrari, A., Sala, P. R., Fasso, A. & Ranft, J. FLUKA: A multi-particle transport code. *CERN-2005-10, INFN/TC_05/11, SLAC-R-773* (2005).
- [37] Agostinelli, S. et al. Geant4 — a simulation toolkit. *Nucl. Instrum. Meth. A*. **506**, 250-303 (2003).
- [38] Sako, T. K. et al. Exploration of a 100 TeV gamma-ray northern sky using the Tibet air-shower array combined with an underground water-Cherenkov muon-detector array. *Astropart. Phys.* **32**, 177-184 (2009).
- [39] Kawata, K. et al. Energy determination of gamma-ray induced air showers observed by an extensive air shower array. *Exp. Astron.* **44**, 1-9 (2017).

- [40] Amenomori, M. et al. Multi-TeV gamma-ray observation from the Crab Nebula using the Tibet-III air shower array finely tuned by the cosmic ray Moon's shadow. *Astrophys. J.* **692**, 61-72 (2009).
- [41] Amenomori, M. et al. Search for gamma rays above 100 TeV from the Crab Nebula with the Tibet air shower array and the 100 m² muon detector. *Astrophys. J.* **813**, 98-102 (2015).
- [42] Li, T.-P. & Ma, Y.-Q. Analysis methods for results in gamma-ray astronomy. *Astrophys. J.* **272**, 317-324 (1983).

Supplementary Information

1 Flux data points of the gamma-ray energy spectrum

The following table shows the flux data points measured by this work along with the detection significance values¹.

Table 1: **Photon flux data points and detection significances for SNR G106.3+2.7.**

Energy (TeV)	Flux ($\text{TeV}^{-1} \text{ cm}^{-2} \text{ s}^{-1}$)	Significance (σ)
6.6	$(1.4 \pm 1.0) \times 10^{-13}$	1.9
11	$(5.6 \pm 2.4) \times 10^{-14}$	2.5
16	$(12.5 \pm 5.7) \times 10^{-15}$	2.3
27	$(3.8 \pm 1.1) \times 10^{-15}$	3.9
45	$(6.2^{+2.4}_{-2.1}) \times 10^{-16}$	3.6
72	$(21.0^{+7.7}_{-6.2}) \times 10^{-17}$	4.9
114	$(2.3^{+2.2}_{-1.4}) \times 10^{-17}$	2.2
184	2.1×10^{-17} (99% U.L.)	–
295	8.3×10^{-18} (99% U.L.)	–

2 Modelling of the multi-wavelength spectrum

We investigate the energy distribution of parent particles (electrons or protons) for gamma-ray emissions from the supernova remnant (SNR) G106.3+2.7 using the *naima* package², which allows us to perform the Markov chain Monte Carlo fitting of radiative models to the observed gamma-ray energy spectrum. We use the data measured by *Fermi*³, VERITAS⁴ and this work in the fitting of the hadronic model. The VERITAS data points are raised by a factor of 1.62 to account for the spill-over of gamma-ray signals outside their window size of 0.32° radius (see Methods of the letter). In the fitting of the leptonic model, we also include the data provided by the Dominion Radio Astrophysical Observatory’s Synthesis Telescope⁵. We assume the distribution of parent particles to have an exponential cutoff power-law form of $dN/dE = AE^{-\alpha}\exp(-E/E_{\text{cut}})$ where A , α and E_{cut} are three fitting parameters. The normalization factor A is replaced by the total energy of parent particles $W_{e/p}$ in the fitting procedure.

2.1 The leptonic scenario

Taking into account the Cosmic Microwave Background (CMB) photons and infrared (IR) photons⁶ with a temperature of 30 K and an energy density of 1 eV cm^{-3} , we attribute the observed gamma-ray energy spectrum to the inverse Compton (IC) scattering of these very low energy photons by relativistic electrons accelerated at the SNR. The best-fit parameters of the parent electron energy distribution are listed in Table 2, and the corresponding gamma-ray energy spectrum is plotted in Figure 4(a). From the fitting results, α and E_{cut} are estimated to be 2.3 and 190 TeV, respectively. The synchrotron cooling time of relativistic electrons is given by $\tau_{\text{syn}} \approx 500 (E/1 \text{ PeV})^{-1} (B/5 \text{ } \mu\text{G})^{-2} \text{ yr}$. For a magnetic field strength $B \sim 8.6 \text{ } \mu\text{G}$, the 190 TeV electrons have $\tau_{\text{syn}} \approx 0.9 \text{ kyr}$, which is much shorter than the SNR age of about 10 kyr. This means that these electrons should be accelerated freshly within a thousand years if they are injected from the SNR.

Another possible source of these electrons is the Boomerang pulsar PSR J2229+6114 and its pulsar wind nebula (PWN), which is 0.44° (or 6 pc at a distance of 0.8 kpc) away from the centroid of observed gamma-ray emissions. The electrons accelerated at the termination shock of this pulsar might be able to diffuse into the gamma-ray emission region. The required total energy of electrons is $\sim 1.4 \times 10^{47} \text{ erg}$, which only takes up $\sim 2\%$ of the spin-down energy released in the entire pulsar lifetime. If the rest of the spin-down energy goes into the magnetic field, the average magnetic field in the PWN would be much larger than the required value of $8 \text{ } \mu\text{G}$ and results in very large fluxes at radio and X-ray wavelengths. The energy budget may be reconciled if the true age of PSR J2229+6114 is much shorter than its characteristic age, say $\sim 1 \text{ kyr}$. In this case, however, it would be difficult to explain the spatial separation between PSR J2229+6114 and the observed γ -ray emission region. The diffusion length is given by $R_d = 2\sqrt{D(E)T}$ [ref. ⁷], where $D(E)$ is the energy-dependent diffusion coefficient that can be expressed as $D(E) = \chi 10^{28} (E/10 \text{ GeV})^{0.5} (B/3 \text{ } \mu\text{G})^{-0.5} \text{ cm}^2 \text{ s}^{-1}$ [ref. ⁸] with a suppression factor χ . Here we simply assume the energy dependence of the average Galactic diffusion coefficient ($D \propto E^{0.5}$), although its validity is not obvious around pulsars. To produce the offset of 0.44° or 6 pc for 190 TeV electrons within their lifetime of $\tau_{\text{syn}} \approx 0.9 \text{ kyr}$, the suppression factor χ should be ~ 0.004 . With these values, 1 TeV electrons that mainly generate $\sim 10 \text{ GeV}$ photons via the IC scattering process diffuse away only by 1.7 pc or $\sim 0.12^\circ$ during the age of 1 kyr. This implies that the GeV gamma-ray emission should be spatially coincident with PSR J2229+6114 rather than the TeV gamma-ray emission, which is inconsistent with the morphology reported by *Fermi*.

In Figure 4(a), the flux of PSR J2229+6114 in the 2–10 keV range⁹ is indicated by the gray open diamond, while an X-ray flux upper limit for the observed gamma-ray emission region has not been measured so far. We emphasize that an upper limit on the synchrotron flux at the X-ray band would provide crucial information to rule out the leptonic scenario as the mechanism of particle acceleration at the source.

2.2 The hadronic scenario

In the hadronic model, γ -rays are produced via proton-proton inelastic collisions to produce π^0 particles which subsequently decay into energetic photons. We assume the proton

density of the target gas³ to be $n_t = 10 \text{ cm}^{-3}$. The best-fit parameters of the parent proton energy distribution are listed in Table 2, and the corresponding gamma-ray energy spectrum is displayed in Figure 4(b). With $E_{\text{cut}} \sim 500 \text{ TeV}$, the proton spectrum has a power-law index of $\alpha \sim 1.8$, falling between the index of the standard diffusive shock acceleration ($\alpha = 2$) and the asymptotic limit of the very efficient proton acceleration^{10,11} ($\alpha = 1.5$). The most likely source of these protons is SNR G106.3+2.7. Generally, SNRs are expected to accelerate protons up to very high energies during their early stage, and the accelerated protons may escape and diffuse away from their acceleration site, resulting in a softened proton energy spectrum. With $\alpha \sim 1.8$, however, the proton energy spectrum does not seem to be softened, which implies that the diffusion may not play a noticeable role. Very likely the protons cannot escape the SNR easily due to the suppression of the diffusion coefficient¹²; while the diffusion length of 500 TeV protons would be 50 pc for $\chi = 0.01$ and $B = 3 \text{ } \mu\text{G}$, protons can be trapped inside a smaller volume comparable to the size of the gamma-ray emission region if $\chi < 0.01$ and/or the true SNR age is shorter than 10 kyr. Alternatively, 500 TeV protons can be confined in an even smaller region of $\sim 5 \text{ pc}$ in radius with a magnetic field of $100 \text{ } \mu\text{G}$ in the extreme case of the Bohm diffusion. The spatially-integrated spectrum of protons trapped inside a small volume would not be modified by the diffusion process.

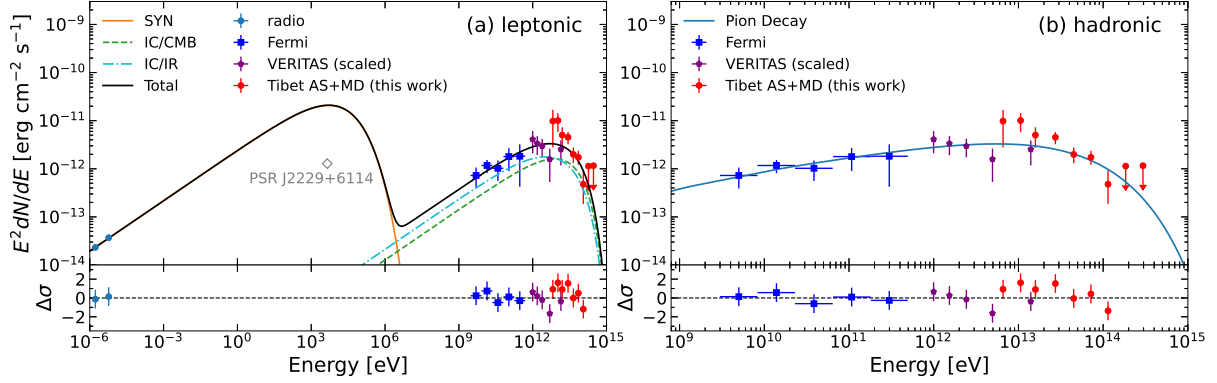


Figure 4: **Spectral gamma-ray energy distribution of G106.3+2.7.** (a) The flux data points with 1σ statistical error bars include measurements by Tibet AS+MD (red dots; this work), *Fermi*³ (blue squares), VERITAS⁴ (purple pentagons) and the Dominion Radio Astrophysical Observatory’s Synthesis Telescope⁵ (turquoise blue dots). The two red downward arrows above 10^{14} eV show 99% C.L. upper limits obtained by this work. Note that all the VERITAS data points are raised by a factor of 1.62 to account for the spill-over of gamma-ray signals outside their window size of 0.32° radius. The best-fit gamma-ray energy spectrum in the leptonic model is shown by the black solid curve, with the flux by the electron synchrotron radiation (the orange solid curve), the IC scattering of CMB photons (the green dashed curve) and the IC scattering of IR photons (the light blue dash-dotted curve). The gray open diamond shows the flux of PSR J2229+6114 obtained in the 2–10 keV range⁹. (b) The best-fit gamma-ray energy spectrum in the hadronic model is shown by the turquoise blue solid curve. The lower panels show the residual $\Delta\sigma$ of the fit.

Table 2: **Best-fit parameters of the energy distribution of parent particles.** Electrons (protons) are assumed for the parent particles of the leptonic (hadronic) model.

	α	E_{cut} (TeV)	$W_{e/p}^\ddagger$ (10^{47} erg)	B (μG)	χ^2/ndf
leptonic	$2.30^{+0.08}_{-0.07}$	190^{+127}_{-66}	$1.4^{+1.8}_{-0.7}$	$8.6^{+3.4}_{-2.5}$	12.8/15
hadronic	$1.79^{+0.08}_{-0.09}$	499^{+382}_{-180}	$5.0^{+0.7}_{-0.6}$	—	13.0/14

[‡] $W_{e/p}$ is the total energy above 10 MeV and 1 GeV for electrons and protons, respectively, where W_p is for a target gas density of 10 cm^{-3} .

References

- [1] Li, T.-P. & Ma, Y.-Q. Analysis methods for results in gamma-ray astronomy. *Astrophys. J.* **272**, 317-324 (1983).
- [2] Zabalza, V. naima: a Python package for inference of relativistic particle energy distributions from observed nonthermal spectra. Preprint at <https://arxiv.org/abs/1509.03319> (2015).
- [3] Xin, Y., Zeng, H., Liu, S., Fan, Y. & Wei, D. VER J2227+608: A hadronic PeVatron pulsar wind nebula? *Astrophys. J.* **885**, 162-167 (2019).
- [4] Acciari, V. A. et al. Detection of extended VHE gamma ray emission from G106.3+2.7 with VERITAS. *Astrophys. J.* **703**, L6-L9 (2009).
- [5] Pineault, S. & Joncas, G. G106.3+2.7: A supernova remnant in a late stage of evolution. *Astron. J.* **120**, 3218-3225 (2000).
- [6] Porter, T. A., Moskalenko, I. V. & Strong, A. W. Inverse Compton emission from galactic supernova remnants: Effect of the interstellar radiation field. *Astrophys. J.* **648**, L29-L32 (2006).
- [7] Aharonian, F. A. & Atoyan, A. M. On the emissivity of π^0 -decay gamma radiation in the vicinity of accelerators of galactic cosmic rays. *Astron. Astrophys.* **309**, 917-928 (1996).
- [8] Gabici, S., Aharonian, F. A. & Casanova, S. Broad-band non-thermal emission from molecular clouds illuminated by cosmic rays from nearby supernova remnants. *Mon. Not. R. Astron. Soc.* **396**, 1629-1639 (2009).
- [9] Halpern, J. P. et al. PSR J2229+6114: Discovery of an energetic young pulsar in the error box of the EGRET source 3EG J2227+6122. *Astrophys. J.* **552**, L125-L128 (2001).
- [10] Malkov, M. A. Asymptotic particle spectra and plasma flows at strong shocks. *Astrophys. J.* **511**, L53-L56 (1999).
- [11] Berezhko, E. G. & Ellison, D. C. A simple model of nonlinear diffusive shock acceleration. *Astrophys. J.* **526**, 385-399 (1999).
- [12] Fujita, Y., Ohira, Y. & Takahara, F. Slow diffusion of cosmic rays around a supernova remnant. *Astrophys. J.* **712**, L153-L156 (2010).